AN ENGINEERING AERODYNAMIC HEATING METHOD FOR HYPERSONIC FLOW

Christopher J. Riley*
NASA Langley Research Center, Hampton, VA

Fred R. DeJarnette†
North Carolina State University, Raleigh, NC

Abstract

A capability to calculate surface heating rates has been incorporated in an approximate three-dimensional inviscid technique. Surface streamlines are calculated from the inviscid solution, and the axisymmetric analog is then used along with a set of approximate convective-heating equations to compute the surface heat transfer. The method is applied to blunted axisymmetric and three-dimensional ellipsoidal cones at angle of attack for the laminar flow of a perfect gas. The method is also applicable to turbulent and equilibrium-air conditions. The present technique predicts surface heating rates that compare favorably with experimental (ground-test and flight) data and numerical solutions of the Navier-Stokes (NS) and viscous shock-layer (VSL) equations. The new technique represents a significant improvement over current engineering aerothermal methods with only a modest increase in computational effort.

Nomenclature

$\mathcal{A}, \mathcal{B}, \mathcal{D}, \mathcal{J}$	geometric factors
$\mathbf{e}_{\bar{s}}, \mathbf{e}_{\bar{t}}$	tangential unit vectors on body surface
$\mathbf{e}_x, \mathbf{e}_r, \mathbf{e}_\phi$	unit vectors of cylindrical coordinate system
$\mathbf{e}_\xi, \mathbf{e}_\beta, \mathbf{e}_n$	unit vectors of shock-oriented coordinate system
$\mathbf{e}_{\bar{\xi}}, \mathbf{e}_{\bar{\beta}}, \mathbf{e}_{\bar{n}}$	unit vectors of streamline coordinate system
f	shock radius
$\bar{f}$	body radius
h_ξ, h_β	scale factors of shock-oriented coordinate system
$h_{\bar{\xi}}, h_{\bar{\beta}}$	scale factors of streamline coordinate system
M	Mach number
n	coordinate normal to shock
$\bar{n}$	coordinate normal to body
p	static pressure
q	heat-transfer rate
R	radius of curvature
u, v, w	velocity components of shock-oriented coordinate system
V	velocity magnitude
$\mathbf{V}$	velocity vector
x, r, ϕ	cylindrical coordinate system
x, y, z	Cartesian coordinate system
α	angle of attack
$,$	shock angle relative to freestream velocity
$\bar{,}$	body angle relative to freestream velocity
δ_ϕ	shock angle in circumferential direction
$\bar{\delta}_\phi$	body angle in circumferential direction
η	stream function ratio, Ψ/Ψ_s
$\bar{\theta}$	inclination angle of surface streamlines
κ_ξ, κ_β	shock curvatures
ξ, β	shock coordinates
$\bar{\xi}, \bar{\beta}$	streamline coordinates
ρ	density
σ	shock angle, $\phi - \delta_\phi$
$\bar{\sigma}$	body angle, $\phi - \bar{\delta}_\phi$
Φ, Ψ	stream functions

Subscripts

b	body
s	shock
w	wall
∞	freestream conditions

Introduction

The thermal design of hypersonic vehicles involves accurately and reliably predicting the convective heating over the surface of the vehicle. Such results may be obtained by numerically solving the Navier-Stokes (NS) equations,[1] or one of their various subsets such as

*Aerospace Technologist, Aerothermodynamics Branch, Space Systems Division. Member AIAA.
†Professor, Mechanical and Aerospace Engineering Department. Associate Fellow AIAA.

Copyright ©1992 by the American Institute of Aeronautics and Astronautics, Inc. No copyright is asserted in the United States under Title 17, U.S. Code. The U.S. Government has a royalty-free license to exercise all rights under the copyright claimed herein for Government purposes. All other rights are reserved by the copyright owner.

the parabolized Navier-Stokes (PNS)[2] and viscous shock-layer (VSL) equations[3,4] for the flowfield surrounding the vehicle. However, due to the excessive computer storage requirements and run times of these detailed approaches, they are impractical for the preliminary design environment where a range of geometries and flow parameters are to be studied. On the other hand, engineering inviscid-viscous methods[5−8] have been demonstrated to adequately predict the heating over a wide range of geometries and aerothermal environments. Various approximations in the inviscid and boundary-layer regions reduce the computer time needed to generate a solution. This reduction in computer time makes the engineering aerothermal methods ideal for parametric studies.

Two of the simpler engineering aerodynamic heating methods that are currently used are AEROHEAT[5,6] and INCHES.[7] Both use the axisymmetric analog concept[9] which allows axisymmetric boundary-layer techniques to be applied to three-dimensional (3-D) flows provided the surface streamlines are known. AEROHEAT calculates approximate surface streamlines based solely on the body geometry. INCHES uses an approximate expression for the scale factor in the windward and leeward planes which describes the spreading of surface streamlines. Circumferential heating rates are then generated by an empirical relation. Another area of approximation is the surface pressure distribution employed by the engineering methods. AEROHEAT assumes modified Newtonian theory which is inaccurate for slender bodies, while INCHES uses an axisymmetric Maslen technique.[10] The deficiencies and limitations of these approximations to the surface streamlines and pressures in the engineering aerothermal methods, along with their corresponding effects on the surface heat transfer, have been documented in Refs. 11 to 13.

An approximate 3-D inviscid method[14,15] has been developed that is more accurate than modified Newtonian theory and has a wider range of applicability than the axisymmetric Maslen technique. The inviscid technique uses two stream functions that approximate the actual stream surfaces in the shock layer and a modified form of the Maslen second-order pressure equation.[16] The method has been shown to calculate the inviscid flowfield about 3-D blunted noses as well as 3-D afterbodies reasonably accurately and much faster than numerical solutions of the inviscid (Euler) equations.[14]

In this paper, the approximate inviscid technique employs the axisymmetric analog to predict laminar and turbulent surface heating rates using the approximate convective-heating equations of Zoby et al.[17] Both perfect gas and equilibrium-air flows are considered. Improved surface streamlines are calculated based on both the body geometry and surface pressure distribution. Surface heating rates are presented for spherically-blunted and asymmetric ellipsoidal cones at angle of attack. Comparisons are made between results of the present technique, VSL and NS solutions, and available experimental data to

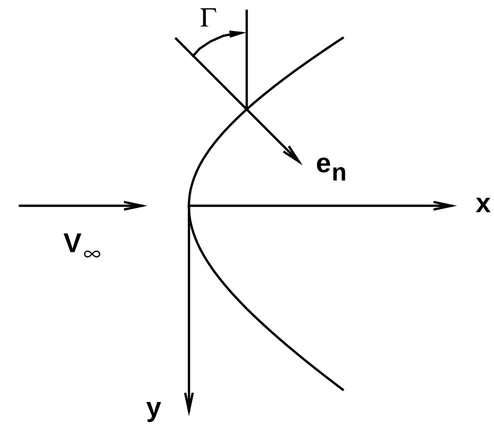

Figure 1. Shock wave geometry: side view.

demonstrate the accuracy and capability of the present engineering technique.

Analysis

This section describes the 3-D inviscid technique, the procedure for computing inviscid surface streamlines, and the application of the axisymmetric analog. Approximations and coupling issues are also discussed.

Inviscid Method

Since a detailed description of the approximate 3-D inviscid method has been presented previously,[14,15] only a brief outline of the inviscid method is given here.

Coordinate Systems

The three-dimensional shock surface can be represented by

$$r_s = f(x, \phi) \tag{1}$$

where (x, r, ϕ) are wind-oriented cylindrical coordinates with corresponding unit vectors $(\mathbf{e}_x, \mathbf{e}_r, \mathbf{e}_\phi)$. The x-axis is aligned with the freestream velocity vector and is normal to the shock surface at the origin. Two angles, $\delta_\phi(x, \phi)$ and , (x, ϕ), describe the shock wave shape and are defined as

$$\tan \delta_\phi = \frac{1}{f}\frac{\partial f}{\partial \phi} \qquad \tan \, , = \frac{\partial f}{\partial x} \cos \delta_\phi \tag{2}$$

An additional angle is given by $\sigma \equiv \phi - \delta_\phi$. All angles are shown in Figs. 1 and 2. For the special case of axisymmetric flow, $r_s = f(x)$, , $=$, (x), $\delta_\phi = 0$, and $\sigma = \phi$.

Next, a shock-oriented curvilinear coordinate system (ξ, β, n) is defined where ξ and β represent coordinates of a point on the shock surface and n is the inward distance normal to the shock. Differential arc lengths along each coordinate direction at the shock are $h_\xi\, d\xi$, $h_\beta\, d\beta$, and

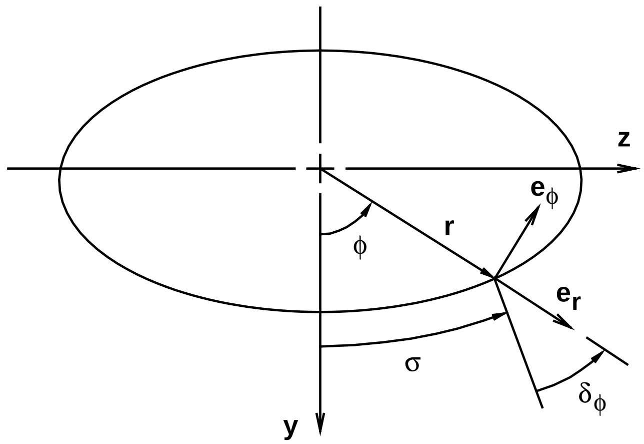

Figure 2. Shock wave geometry: rear view.

dn where h_ξ and h_β are scale factors for the corresponding coordinates. This coordinate system is well-suited for hypersonic flow ($M_\infty \gg 1$) and thin shock layers.

The unit vectors, $\mathbf{e}_\xi$ and $\mathbf{e}_\beta$, are tangent to the shock surface and are chosen such that $\mathbf{e}_\xi$ is in the direction of the tangential velocity just inside the shock surface. The unit vector $\mathbf{e}_\beta$ is then defined to be perpendicular to $\mathbf{e}_\xi$ and $\mathbf{e}_n$. In cylindrical coordinates, the unit vectors of the curvilinear coordinate system are given by

$$\begin{aligned}
\mathbf{e}_\xi &= \cos,\ \mathbf{e}_x + \sin,\ (\cos\delta_\phi\, \mathbf{e}_r - \sin\delta_\phi\, \mathbf{e}_\phi) \\
\mathbf{e}_\beta &= \sin\delta_\phi\, \mathbf{e}_r + \cos\delta_\phi\, \mathbf{e}_\phi \qquad (3) \\
\mathbf{e}_n &= \sin,\ \mathbf{e}_x - \cos,\ (\cos\delta_\phi\, \mathbf{e}_r - \sin\delta_\phi\, \mathbf{e}_\phi)
\end{aligned}$$

Although this curvilinear coordinate system is orthogonal at the shock surface, it is nonorthogonal within the shock layer for a general three-dimensional shock. However, for thin shock layers, orthogonality may be assumed everywhere.

The velocity is defined in terms of the unit vectors at the shock as

$$\mathbf{V} = u\mathbf{e}_\xi + v\mathbf{e}_n + w\mathbf{e}_\beta \qquad (4)$$

From the definition of $\mathbf{e}_\xi$ and $\mathbf{e}_\beta$, the crossflow velocity component at the shock, w_s, is equal to zero.

Governing Equations

The governing equations for 3-D inviscid flow are simplified by assuming that the velocity component w is equal to zero not only at the shock but throughout the shock layer. This yields two stream functions, Φ (which is equal to β here) and Ψ, which approximate the actual stream surfaces in the shock layer. The stream function Ψ is analogous to the Stokes stream function for axisymmetric flow.

Approximate expressions for the pressure and normal velocity component are then obtained by transforming the normal momentum and continuity equations to streamline coordinates and evaluating the flow variables at the shock. Along a line normal to the shock, these expressions are

$$\begin{aligned}
p(\eta) &= p_s + p_1(\eta - 1) + p_2(\eta^2 - 1) \qquad (5) \\
v(\eta) &= v_s + v_1(\eta - 1) \qquad (6)
\end{aligned}$$

where

$$\begin{aligned}
p_1 &= \frac{\Psi_s u_s \kappa_\xi}{h_\beta} \\
p_2 &= -\frac{\Psi_s v_s \tan,}{2h_\beta}(\kappa_\xi + \kappa_\beta) \\
v_1 &= \frac{\Psi_s v_s}{h_\beta \cos,}(\kappa_\xi + \kappa_\beta)
\end{aligned}$$

and

$$\eta = \frac{\Psi}{\Psi_s}$$

Defining $\Psi = 0$ to be the body surface gives $\eta = 1$ on the shock and $\eta = 0$ on the body. Note that Eq. (5) reduces to Maslen's second-order pressure equation[16] for axisymmetric flow if the scale factor h_β is equal to the shock radius r_s.

Method of Solution

Since the inviscid method is an inverse one, the shock shape must be varied until the correct body shape is produced. The resulting iteration procedure is handled differently in each region of the flow.

In the stagnation region of a blunt body traveling at hypersonic speeds, the flow is subsonic and the shock shape for the entire subsonic-transonic region must be determined globally. A 3-D shock given by longitudinal conic sections blended in the circumferential direction with an ellipse is assumed. The parameters describing the shock are iterated until the body shape ($\Psi = 0$) generated by the approximate inviscid method matches the actual body shape at several discrete points. In this study, six shock parameters are varied until the calculated body is matched to the actual body at six locations.

Once past the transonic region, the inviscid flow is totally supersonic and a marching scheme is well posed. The shock surface from the transonic region forms a starting solution for the marching procedure. The shock variables are extrapolated in ξ along a number of constant β lines which circle the shock. On each line, the shock curvature κ_ξ is locally iterated until the calculated body shape matches the correct body. The shock variables are then advanced downstream to the next ξ-location and the process repeated.

Axisymmetric Analog

The 3-D boundary-layer analysis is simplified by using the axisymmetric analog[9] as is done in most engineering aerothermal methods. The 3-D boundary-layer equations are first written in a streamline coordinate system. The crossflow velocity component tangent to the surface but normal to the streamline is then assumed to be zero. This simplification reduces the 3-D boundary-layer equations to the axisymmetric form provided the distance along the streamline is substituted for the surface distance and the scale factor describing the divergence of the streamlines is interpreted as the axisymmetric body radius. Axisymmetric boundary-layer methods can then be employed in the existing 3-D inviscid technique.

Inviscid Surface Streamlines

Before applying the axisymmetric analog, inviscid surface streamlines are computed from the approximate inviscid solution. Inviscid surface streamlines may be calculated from the surface pressure distribution[5] or from the velocity components.[8] The approximate inviscid method[14,15] used here predicts accurate surface pressures, but the direction of the velocity on the surface is not accurate. Therefore, in the present method, streamlines are calculated from the surface pressures.

A streamline coordinate system[5] $(\bar{\xi}, \bar{\beta}, \bar{n})$ is defined where $\bar{\xi}$ and $\bar{\beta}$ are coordinates of a point on the body surface and $\bar{n}$ is the distance normal to the body. The bars indicate the variables apply to the body and not the shock. Differential arc lengths along each coordinate direction at the body are $h_{\bar{\xi}}\, d\bar{\xi}$, $h_{\bar{\beta}}\, d\bar{\beta}$, and $d\bar{n}$ where $h_{\bar{\xi}}$ and $h_{\bar{\beta}}$ are scale factors for the corresponding coordinates. If the body surface is represented by $r_b = \bar{f}(x, \phi)$ in wind axes with the axial coordinate parallel to the freestream velocity and passing through the stagnation point, the unit vector normal (outward) to the body surface is given by

$$\mathbf{e}_{\bar{n}} = -\sin\bar{\Gamma}\, \mathbf{e}_x + \cos\bar{\Gamma}\, (\cos\bar{\delta}_\phi\, \mathbf{e}_r - \sin\bar{\delta}_\phi\, \mathbf{e}_\phi) \tag{7}$$

The body angles are defined in the same fashion as the shock angles and are

$$\tan\bar{\delta}_\phi = \frac{1}{\bar{f}}\frac{\partial \bar{f}}{\partial \phi} \qquad \tan\bar{\Gamma} = \frac{\partial \bar{f}}{\partial x}\cos\bar{\delta}_\phi \tag{8}$$

The tangential unit vectors at the surface, $\mathbf{e}_{\bar{\xi}}$ and $\mathbf{e}_{\bar{\beta}}$, are similar to the tangential unit vectors at the shock. From Ref. 5, they are given as

$$\mathbf{e}_{\bar{\xi}} = \cos\bar{\theta}\, \mathbf{e}_{\bar{s}} + \sin\bar{\theta}\, \mathbf{e}_{\bar{t}} \tag{9}$$

$$\mathbf{e}_{\bar{\beta}} = -\sin\bar{\theta}\, \mathbf{e}_{\bar{s}} + \cos\bar{\theta}\, \mathbf{e}_{\bar{t}} \tag{10}$$

where

$$\mathbf{e}_{\bar{s}} = \cos\bar{\Gamma}\, \mathbf{e}_x + \sin\bar{\Gamma}\, (\cos\bar{\delta}_\phi\, \mathbf{e}_r - \sin\bar{\delta}_\phi\, \mathbf{e}_\phi) \tag{11}$$

$$\mathbf{e}_{\bar{t}} = \sin\bar{\delta}_\phi\, \mathbf{e}_r + \cos\bar{\delta}_\phi\, \mathbf{e}_\phi \tag{12}$$

and the angle $\bar{\theta}$ represents the orientation of the surface streamlines. Note that the vectors, $\mathbf{e}_{\bar{s}}$ and $\mathbf{e}_{\bar{t}}$, are identical in form to the unit vectors, $\mathbf{e}_\xi$ and $\mathbf{e}_\beta$, defined at the shock.

The orientation of the inviscid surface streamlines, given by $\bar{\theta}$, is found by applying the momentum equations along the body surface using the pressure distribution generated by the inviscid solution. By writing the momentum equations in streamline coordinates, taking the scalar product with $\mathbf{e}_{\bar{\beta}}$, and substituting the unit vectors, Eqs. (9) and (10), this may be expressed as

$$\frac{1}{h_{\bar{\xi}}}\frac{\partial \bar{\theta}}{\partial \bar{\xi}} = -\frac{\sin\bar{\Gamma}}{h_{\bar{\xi}}}\frac{\partial \bar{\sigma}}{\partial \bar{\xi}} - \frac{1}{\rho_b V_b^2}\frac{1}{h_{\bar{\beta}}}\frac{\partial p_b}{\partial \bar{\beta}} \tag{13}$$

where $\bar{\sigma} \equiv \phi - \bar{\delta}_\phi$. The scale factor $h_{\bar{\beta}}$ can be determined by noting that for an orthogonal curvilinear coordinate system

$$\frac{\partial}{\partial \bar{\xi}}\left(h_{\bar{\beta}}\mathbf{e}_{\bar{\beta}}\right) = \frac{\partial}{\partial \bar{\beta}}\left(h_{\bar{\xi}}\mathbf{e}_{\bar{\xi}}\right)$$

Taking the scalar product of this equation with $\mathbf{e}_{\bar{\beta}}$ and again substituting the unit vectors, Eqs. (9) and (10), yields

$$\frac{1}{h_{\bar{\xi}}}\frac{\partial \ln h_{\bar{\beta}}}{\partial \bar{\xi}} = \frac{1}{h_{\bar{\beta}}}\frac{\partial \bar{\theta}}{\partial \bar{\beta}} + \frac{\sin\bar{\Gamma}}{h_{\bar{\beta}}}\frac{\partial \bar{\sigma}}{\partial \bar{\beta}} \tag{14}$$

Equations (13) and (14) may be integrated along a surface streamline to obtain the streamline direction $\bar{\theta}$ and the scale factor $h_{\bar{\beta}}$. Although the surface streamlines can be determined after the inviscid solution has already been calculated, it was found to be more convenient to compute the inviscid solution and the surface streamlines simultaneously. Before applying these equations along shock coordinates, transformation operators relating derivatives with respect to the the streamline coordinates $(\bar{\xi}, \bar{\beta})$ to derivatives with respect to the shock coordinates (ξ, β) are needed. In the approximate inviscid method, the curvilinear coordinate system is assumed to be orthogonal throughout the shock layer. This assumption simplifies the analysis but does not change the form of the approximate pressure and velocity relations, Eqs. (5) and (6), since the flowfield variables are evaluated at the shock where the coordinate system is orthogonal. However, at the body surface, the correct coordinate directions need to be considered. Following the approach of Ref. 15 and using the nonorthogonal directions at the surface, the transformation operators are

$$\begin{aligned}\frac{\mathcal{J}}{h_{\bar{\xi}}}\frac{\partial}{\partial \bar{\xi}} &= \left(\mathcal{B}\mathbf{e}_{\bar{\xi}} \cdot \mathbf{e}_\xi - \mathcal{D}\mathbf{e}_{\bar{\xi}} \cdot \mathbf{e}_\beta\right)\frac{1}{h_\xi}\frac{\partial}{\partial \xi} \\ &+ \left(-\mathcal{D}\mathbf{e}_{\bar{\xi}} \cdot \mathbf{e}_\xi + \mathcal{A}\mathbf{e}_{\bar{\xi}} \cdot \mathbf{e}_\beta\right)\frac{1}{h_\beta}\frac{\partial}{\partial \beta}\end{aligned} \tag{15}$$

and

$$\begin{aligned}\frac{\mathcal{J}}{h_{\bar{\beta}}}\frac{\partial}{\partial \bar{\beta}} &= \left(\mathcal{B}\mathbf{e}_{\bar{\beta}} \cdot \mathbf{e}_\xi - \mathcal{D}\mathbf{e}_{\bar{\beta}} \cdot \mathbf{e}_\beta\right)\frac{1}{h_\xi}\frac{\partial}{\partial \xi} \\ &+ \left(-\mathcal{D}\mathbf{e}_{\bar{\beta}} \cdot \mathbf{e}_\xi + \mathcal{A}\mathbf{e}_{\bar{\beta}} \cdot \mathbf{e}_\beta\right)\frac{1}{h_\beta}\frac{\partial}{\partial \beta}\end{aligned} \tag{16}$$

where

$$\mathcal{A} = 1 - n_b\kappa_\xi$$

$$\mathcal{B} = 1 - n_b \kappa_\beta$$
$$\mathcal{D} = \frac{n_b}{h_\beta}\frac{\partial,}{\partial \beta}$$
$$\mathcal{J} = \mathcal{A}\mathcal{B} - \mathcal{D}^2$$

These operators can be used to calculate the pressure derivative in Eq. (13) as well as allow Eqs. (13) and (14) to be integrated with respect to the shock coordinate ξ.

Boundary-Layer Method

The axisymmetric analog allows any axisymmetric boundary-layer method to be applied along an inviscid surface streamline. In this study, a set of approximate convective-heating equations developed by Zoby et al.[17] is used for the boundary-layer solution. Laminar and turbulent heating rates may be calculated from these relations for both perfect gas and equilibrium-air flows. Approximate expressions for the boundary-layer thickness at both laminar and turbulent conditions are also given in Ref. 17. Results using this technique have been shown to compare favorably with more detailed methods for wind tunnel and flight conditions.[18–20] Boundary-layer edge conditions are found by interpolating in the approximate inviscid solution a distance away from the wall equal to the boundary-layer thickness. This approach has been demonstrated to approximately account for the effects of entropy-layer swallowing.

Results and Discussion

Surface heating rates are presented at perfect gas and laminar conditions over spherically-blunted and 3-D ellipsoidal cones at angle of attack in order to demonstrate the capability and accuracy of the present technique. A comparison with flight data obtained at laminar and turbulent flow conditions is also presented based on equilibrium-air calculations.

Spherically-Blunted Cones

Computed laminar surface heating rates are presented in Figs. 3 and 4 for the windward plane of a 15 deg spherically-blunted cone at angles of attack of 5 and 10 deg. The freestream Mach number is 10.6 and the nose radius is 1.1 inches. Results of the present method are compared with results of an engineering aerothermal method AEROHEAT[5,6] and experimental data.[21] Good agreement (within 10 percent) between the results of the present method and the experimental data is shown in Figs. 3 and 4. The AEROHEAT results fail to predict the correct magnitude of the surface heating as well as the local maximum in the heating. These discrepancies can be attributed to the approximate pressure distribution and streamlines used in AEROHEAT. Circumferential heating rates are presented in Figs. 5 and 6 at two

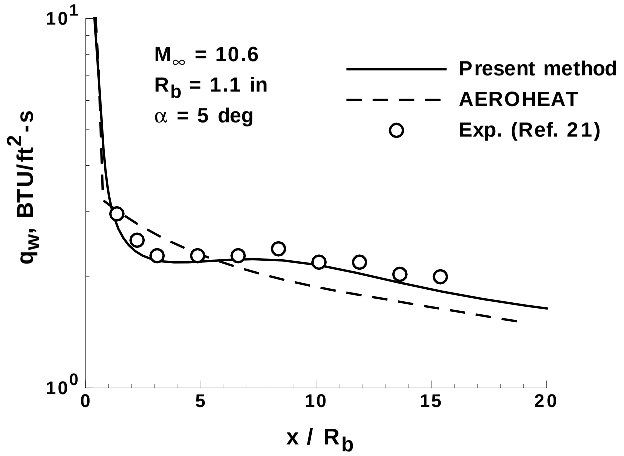

Figure 3. Comparison of surface heating rates for 15 deg sphere-cone.

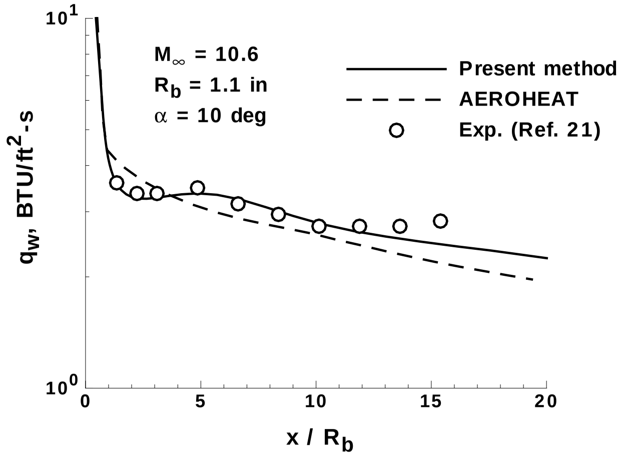

Figure 4. Comparison of surface heating rates for 15 deg sphere-cone.

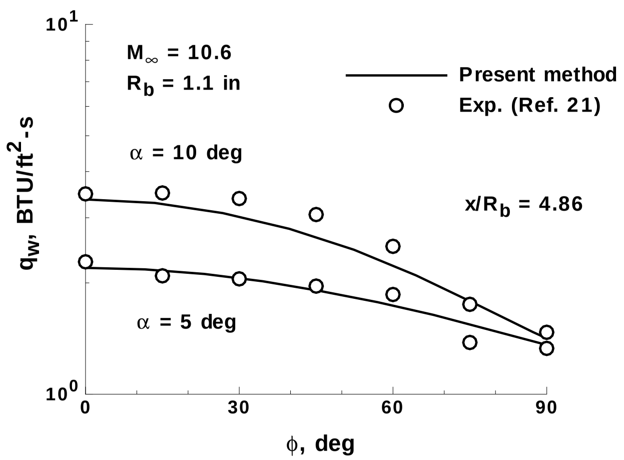

Figure 5. Comparison of circumferential surface heating rates for 15 deg sphere-cone.

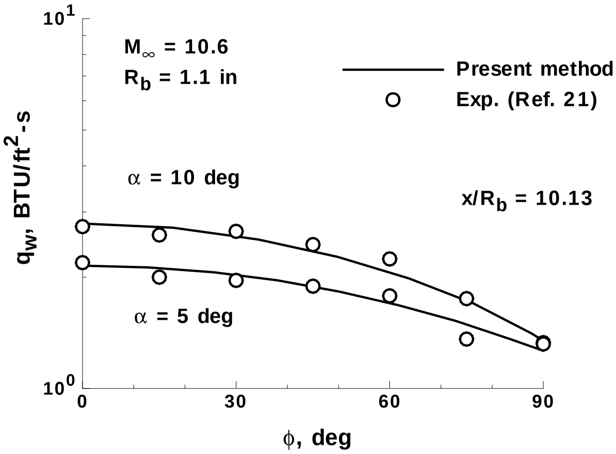

Figure 6. Comparison of circumferential surface heating rates for 15 deg sphere-cone.

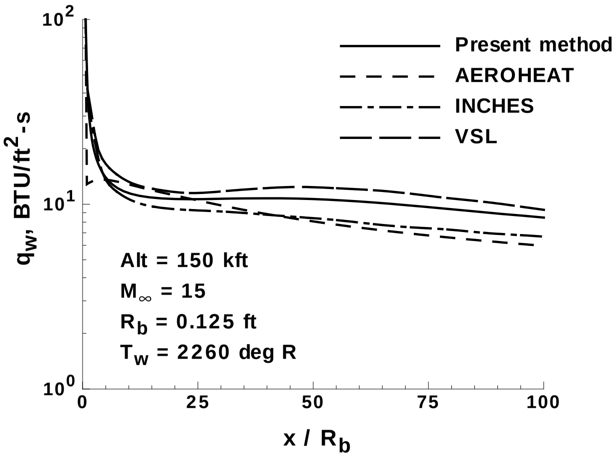

Figure 7. Comparison of surface heating rates for 5 deg sphere-cone at $\alpha = 3$ deg.

axial locations on the blunted cone for angles of attack of 5 and 10 deg. The windward plane is located at $\phi = 0$ deg and the side plane is at $\phi = 90$ deg. The comparison of the experimental and predicted heating rates is seen to be good at both axial stations of 4.86 and 10.13 nose radii. This comparison illustrates that the present technique is capable of computing heating rates off the windward plane of symmetry.

In order to demonstrate the significant improvement of the present method over current engineering aerodynamic heating methods, the surface heating rates in the windward plane of symmetry are calculated for a 5 deg spherically-blunted cone at an angle of attack of 3 deg. The freestream Mach number is 15 and the freestream conditions correspond to an altitude of 150,000 ft. The wall temperature is 2260 deg R and the nose radius is 0.125 ft. Heating rates are computed using the present technique, AEROHEAT, INCHES,[7] and a detailed VSL method.[11] The resulting surface heating rates are presented in Fig. 7. The surface heating rates generated by AEROHEAT and INCHES differ by as much as 40 percent from the more accurate VSL solution. On the other

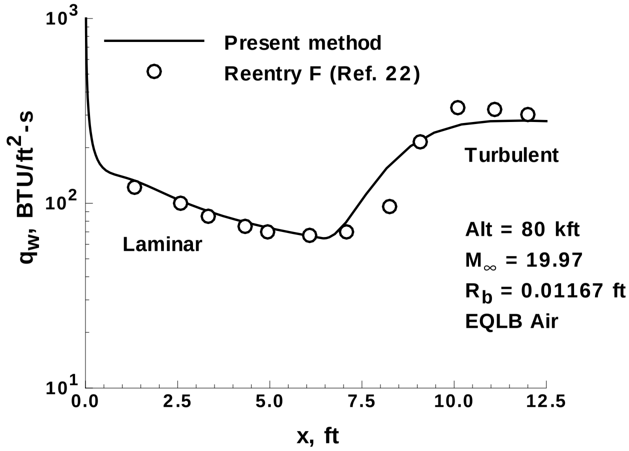

Figure 8. Comparison of surface heating rates with Reentry F flight data (5 deg sphere-cone at $\alpha = 0.14$ deg).

hand, the solution of the present method shows much better agreement (within 15 percent) with the VSL results and also predicts the correct trend in the surface heating rate levels.

The surface heating rates over a 5 deg spherically-blunted cone at equilibrium-air and turbulent conditions are examined next in Fig. 8. Results from the present method are compared with heat-transfer data obtained from the flight experiment Reentry F.[22] The Reentry F vehicle was a 5 deg spherically-blunted cone with a length of 13 ft and an initial nose radius of 0.1 inches. The data shown in Fig. 8 correspond to a trajectory point at 80,000 ft. The freestream Mach number is approximately 20 and the angle of attack is 0.14 deg. The results depicted correspond to the leeward plane of the vehicle. In the present technique, equilibrium air properties are obtained from Hansen,[23] while transition is assumed to begin at the reported distance.[22] The calculated heating rates in the transition region are based on the Dhawan and Narasimha[24] model. Excellent comparison between the results from the present technique and the flight laminar and turbulent data is noted.

Ellipsoidal Cones

The perfect gas, laminar solution over a blunted 2:1 ellipsoidal cone is examined next at angles of attack of 0 and 15 deg. The cone angles in the windward and side planes are 5 and 9.93 deg, respectively. The freestream Mach number is 10.19 and the nose radius in the side plane is 1.0 inch. Surface heating rates from the present technique are compared with results from a NS method, LAURA,[1] and experimental data.[25] The LAURA method is chosen for comparison purposes because of its ability to compute the flowfield about a 3-D nose. In addition, there is an apparent lack of heat-transfer data available in the open literature on 3-D nose shapes. Thirty-seven streamlines are used to obtain the solution around the

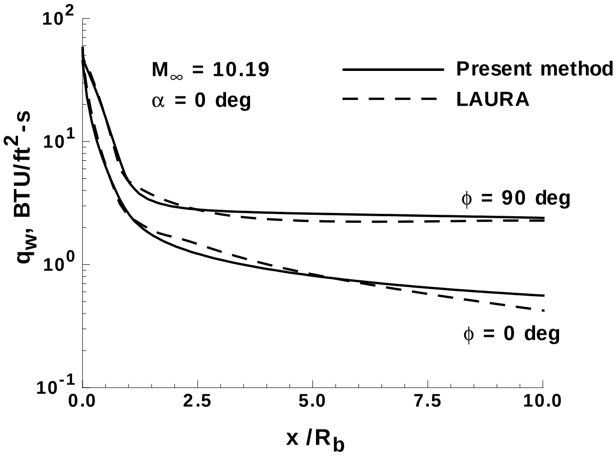

Figure 9. Comparison of surface heating rates for 2:1 ellipsoidal cone.

ellipsoidal cone in the present technique. A grid of 64 cells in the axial direction, 30 cells around the circumference of the body, and 64 cells in the normal direction is used to obtain the LAURA solution. The present technique requires approximately 200 CPU sec on a Sun workstation to obtain a solution, while the LAURA solution requires approximately 4 CPU hrs on a CRAY-2 supercomputer. No effort was made to optimize the LAURA calculations.

Axial surface heating rates are depicted in Fig. 9 for the windward ($\phi = 0$ deg) and side ($\phi = 90$ deg) planes at an angle of attack of 0. Good agreement is noted near the nose and in the side plane downstream. However, in the windward plane downstream, the results from the present technique overestimate the results generated by LAURA by 25 percent. For the ellipsoidal cone, the surface streamlines diverge rapidly from the side plane and converge towards the windward plane. Unfortunately, in this inflow region near the windward plane, it appears that the approximate surface pressures are not accurate enough to predict reasonable streamline paths. For this reason, the solution over the ellipsoidal cone at 0 deg angle of attack is computed using simplified surface streamlines by setting the streamline angle $\bar{\theta}$ equal to zero. Accounting for the inflow correctly downstream would reduce the heating rates near the windward plane. However, at angle of attack, the streamlines are again computed using the surface pressures since the inflow is reduced.

Circumferential heating rates for the ellipsoidal cone at 0 deg angle of attack are depicted in Figs. 10 – 13 at four axial locations on the body. The first is on the 3-D nose, while the remaining three are downstream on the 3-D afterbody. Excellent agreement (within 10 percent) is seen at $x/R_b = 0.4$ on the 3-D nose. At $x/R_b = 2.2$, the rapid drop in the heating rate away from the side plane may be attributed to the fact that the approximate inviscid solution is based on the shock and tends to smooth the effects of the discontinuity in body curvature at the nose-afterbody juncture. The same trend was noted in the pressure comparisons in Ref. 14. This effect is seen

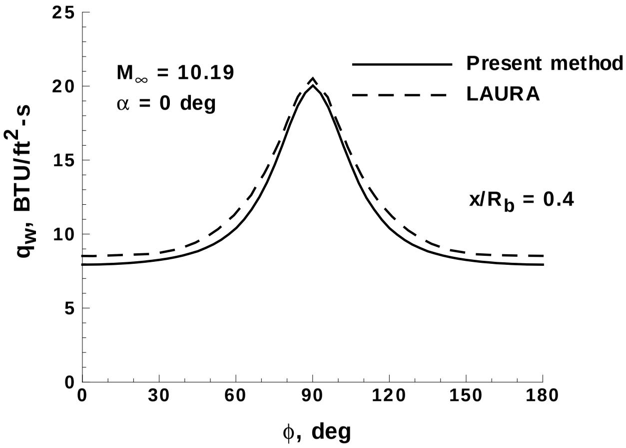

Figure 10. Comparison of circumferential surface heating rates for 2:1 ellipsoidal cone.

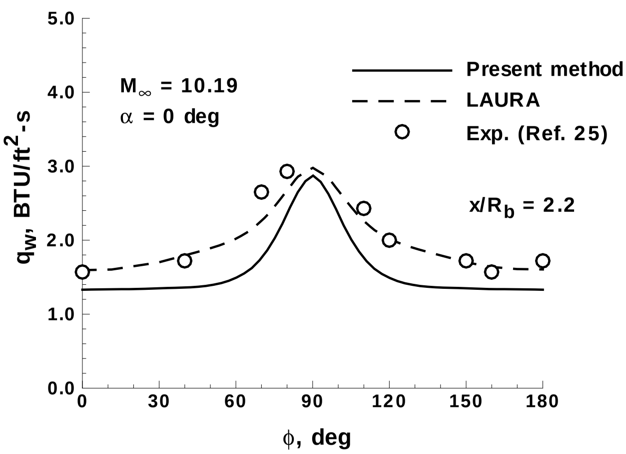

Figure 11. Comparison of circumferential surface heating rates for 2:1 ellipsoidal cone.

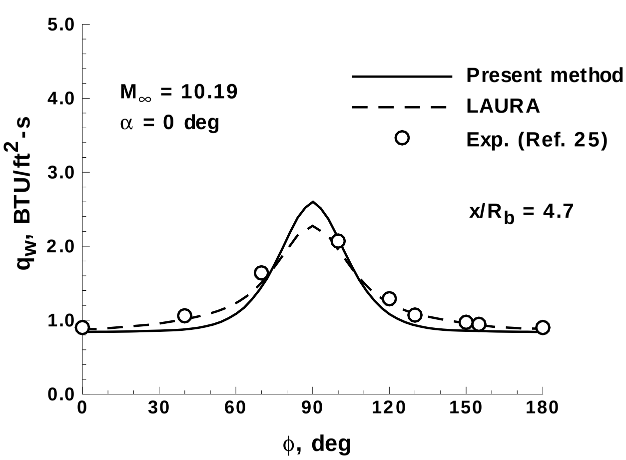

Figure 12. Comparison of circumferential surface heating rates for 2:1 ellipsoidal cone.

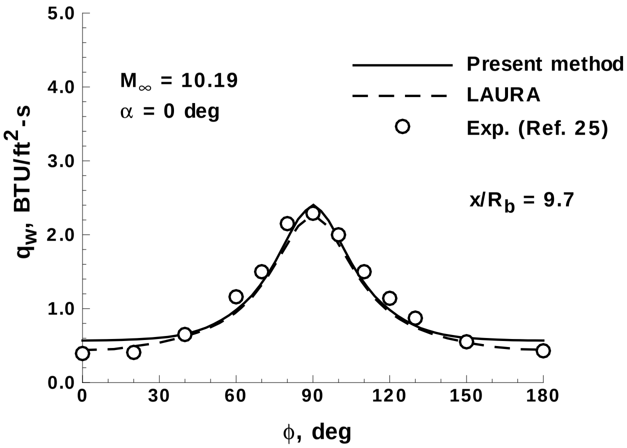

Figure 13. Comparison of circumferential surface heating rates for 2:1 ellipsoidal cone.

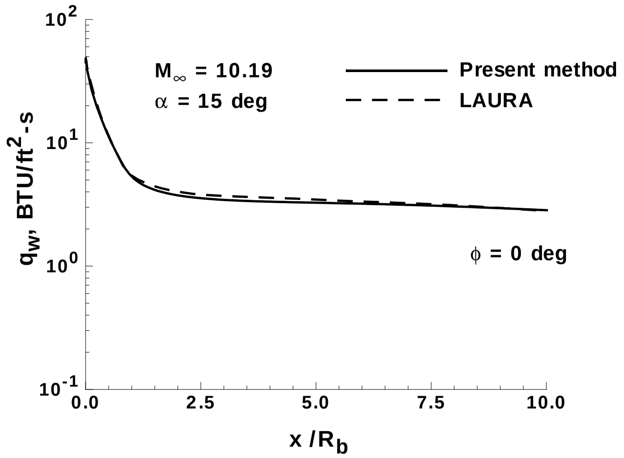

Figure 14. Comparison of surface heating rates for 2:1 ellipsoidal cone.

in Fig. 9 around $x/R_b = 1.0$. However, farther downstream at $x/R_b = 9.7$ in Fig. 13, the surface heating rates from the present method match the circumferential distribution of the LAURA solution and the experimental data except near the windward and leeward planes.

The axial surface heating rates in the windward plane on the 2:1 ellipsoidal cone at 15 deg angle of attack is shown in Fig. 14. The agreement between the present results and the LAURA solution is excellent. As noted previously, surface streamlines are computed from the pressure distribution at angle of attack. Circumferential surface heating rates are depicted in Figs. 15 – 18 at the same four axial locations as shown for the 0 deg angle-of-attack case. The present technique is inappropriate for calculations in the viscous-dominated leeward region of a body at angle of attack. For this reason, the solution is computed in the windward region only ($\phi < 90$ deg). Good agreement (within 15 percent) is noted both on the 3-D nose and at the axial stations downstream. There are some discrepancies between the results from LAURA and the experimental data at $x/R_b = 9.7$. However, these comparisons not only demonstrate an improved capability

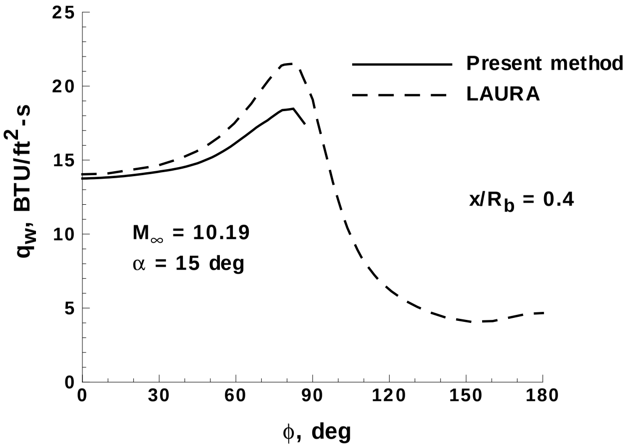

Figure 15. Comparison of circumferential surface heating rates for 2:1 ellipsoidal cone.

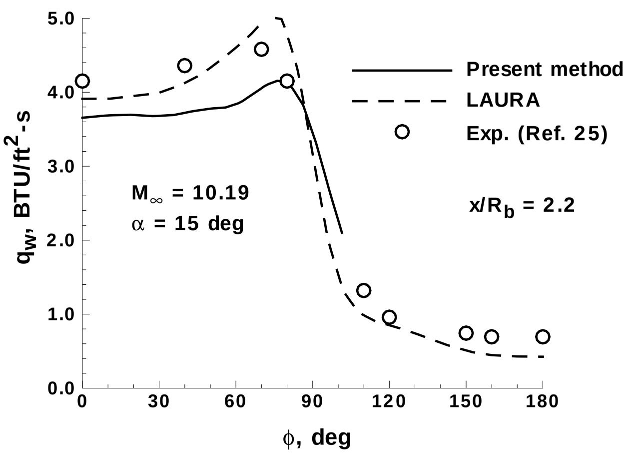

Figure 16. Comparison of circumferential surface heating rates for 2:1 ellipsoidal cone.

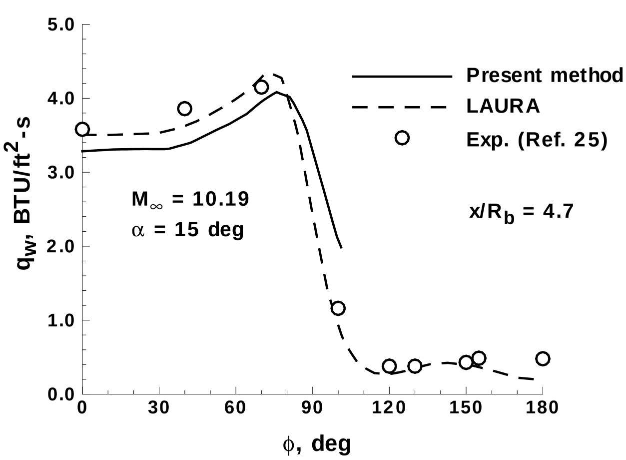

Figure 17. Comparison of circumferential surface heating rates for 2:1 ellipsoidal cone.

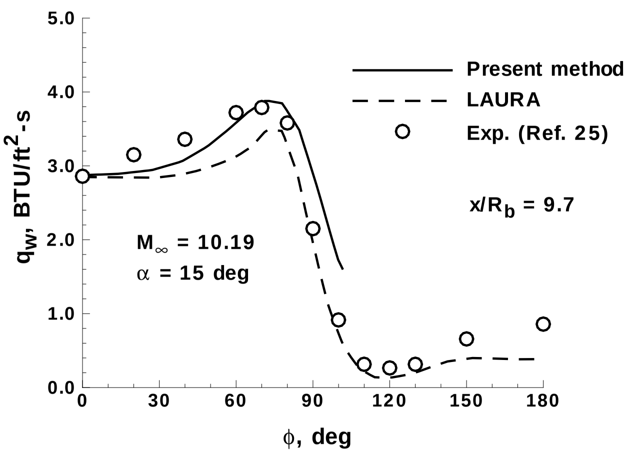

Figure 18. Comparison of circumferential surface heating rates for 2:1 ellipsoidal cone.

over present engineering methods, but the applications to 3-D bodies significantly enhance current capabilities.

Concluding Remarks

A rapid but reliable engineering aerodynamic heating method has been developed by coupling an approximate 3-D inviscid technique with the axisymmetric analog and a set of approximate convective-heating equations. Surface streamlines are calculated using both the body geometry and surface pressure distribution. The method is applied to the solution over spherically-blunted cones and 3-D ellipsoidal cones at angle of attack for the laminar and turbulent flow of a perfect gas and equilibrium air. The present technique predicts surface heating rates that compare favorably with experimental data, equilibrium-air flight data, and numerical solutions of the NS and VSL equations. It also represents a significant improvement over current engineering aerothermal methods with only a modest increase in computational effort.

Acknowledgements

Research performed by the second author was supported by Cooperative Agreement NCC1-100 with the Aerothermodynamics Branch of the Space Systems Division at NASA Langley Research Center. The authors wish to thank Mr. E. Vincent Zoby, Dr. Peter A. Gnoffo, and Mr. H. Harris Hamilton of the Aerothermodynamics Branch and Dr. F. McNeil Cheatwood of North Carolina State University for their guidance and assistance.

References

[1]Gnoffo, P. A., "An Upwind-Biased, Point-Implicit Relaxation Algorithm for Viscous, Compressible Perfect-Gas Flows," NASA TP-2953, Feb. 1990.

[2]Lawrence, S. L., Chaussee, D. S., and Tannehill, J. C., "Application of an Upwind Algorithm to the Three-Dimensional Parabolized Navier-Stokes Equations," AIAA Paper 87-1112-CP, June 1987.

[3]Thompson, R. A., "Comparison of Nonequilibrium Viscous-Shock-Layer Solutions with Shuttle Heating Measurements," *Journal of Thermophysics and Heat Transfer*, Vol. 4, April 1990, pp. 162–169.

[4]Swaminathann, S., Kim, M. D., and Lewis, C. H., "Three-Dimensional Nonequilibrium Viscous Shock-Layer Flows Over Complex Geometries," AIAA Paper 83-0212, Jan. 1983.

[5]DeJarnette, F. R. and Hamilton, H. H., "Inviscid Surface Streamlines and Heat Transfer on Shuttle-Type Configurations," *Journal of Spacecraft and Rockets*, Vol. 10, May 1973, pp. 314–321.

[6]DeJarnette, F. R. and Hamilton, H. H., "Aerodynamic Heating on 3-D Bodies Including the Effects of Entropy-Layer Swallowing," *Journal of Spacecraft and Rockets*, Vol. 12, Jan.-Feb. 1975, pp. 5–12.

[7]Zoby, E. V. and Simmonds, A. L., "Engineering Flowfield Method With Angle-of-Attack Applications," *Journal of Spacecraft and Rockets*, Vol. 22, July-Aug. 1985, pp. 398–405.

[8]Hamilton, H. H., DeJarnette, F. R., and Weilmuenster, K. J., "Application of Axisymmetric Analog for Calculating Heating in Three-Dimensional Flows," *Journal of Spacecraft and Rockets*, Vol. 24, July-Aug. 1987, pp. 296–302.

[9]Cooke, J. C., "An Axially Symmetric Analogue for General Three-Dimensional Boundary Layers," British Ministry of Aviation, Aeronautical Research Council TR, R&M 3200, June 1961.

[10]Zoby, E. V. and Graves, R. A., Jr., "A Computer Program for Calculating the Perfect Gas Inviscid Flow Field About Blunt Axisymmetric Bodies at an Angle of Attack of 0 deg," NASA TM X-2843, Dec. 1973.

[11]Thompson, R. A., Zoby, E. V., Wurster, K. E., and Gnoffo, P. A., "An Aerothermodynamic Study of Slender Conical Vehicles," *Journal of Thermophysics and Heat Transfer*, Vol. 3, Oct. 1990, pp. 361–367.

[12]Riley, C. J., DeJarnette, F. R., and Zoby, E. V., "Surface Pressure and Streamline Effects on Laminar Heating Calculations," *Journal of Spacecraft and Rockets*, Vol. 27, Jan.-Feb. 1990, pp. 9–14.

[13]Wurster, K. E., Zoby, E. V., and Thompson, R. A., "Influence of Flowfield and Vehicle Parameters on Engineering Aerothermal Methods," AIAA Paper 89-1769, June 1989.

[14]Riley, C. J. and DeJarnette, F. R., "Engineering Calculations of Three-Dimensional Inviscid Hypersonic Flow Fields," AIAA Paper 91-0701, Jan. 1990.

[15]Riley, C. J. and DeJarnette, F. R., "An Approximate Method for Calculating Three-Dimensional Inviscid Hypersonic Flow Fields," NASA TP-3018, Aug. 1990.

[16]Maslen, S. H., "Asymmetric Hypersonic Flow," NASA CR-2123, Sept. 1972.

[17]Zoby, E. V., Moss, J. N., and Sutton, K., "Approximate Convective-Heating Equations for Hypersonic Flows," *Journal of Spacecraft and Rockets*, Vol. 18, Jan.-Feb. 1981, pp. 64–70.

[18]Zoby, E. V., "Approximate Heating Analysis for the Windward Symmetry Plane of Shuttle-Like Bodies at Large Angle of Attack," *Progress in Astronautics and Aeronautics*, Vol. 82, edited by T. E. Horton, AIAA, New York, 1982, pp. 229–247.

[19]Zoby, E. V., "Comparisons of STS-1 Experimental and Predicted Heating Rates," *Journal of Spacecraft and Rockets*, Vol. 20, May-June 1983, pp. 214–218.

[20]Zoby, E. V., "Analysis of STS-2 Experimental Heating Rates and Transition Data," *Journal of Spacecraft and Rockets*, Vol. 20, May-June 1983, pp. 232–237.

[21]Cleary, J. W., "Effects of Angle of Attack and Bluntness on Laminar Heating-Rate Distributions of a 15^o Cone at a Mach Number of 10.6," NASA TN D-5450, Oct. 1969.

[22]Stainback, P. C., Johnson, C. B., Boney, L. B., and Wicker, K. C., "Comparison of Theoretical Predictions and Heat-Transfer Measurements for a Flight Experiment at Mach 20 (Reentry F)," NASA TM X-2560, 1972.

[23]Hansen, C. F., "Approximations for the Thermodynamic and Transport Properties of High-Temperature Air," NASA TR R-50, 1959.

[24]Dhawan, S. and Narasimha, R., "Some Properties of Boundary Layer Flow During Transition from Laminar to Turbulent Motion," *Journal of Fluid Mechanics*, Vol. 3, April 1958, pp. 418–436.

[25]Hillsamer, M. E. and Rhudy, J. P., "Heat-Transfer and Shadowgraph Tests of Several Elliptical Lifting Bodies at Mach 10," AEDC-TDR-64-19, Feb. 1964.